Analysis of the coupling of light into a metal–dielectric composite waveguide structure and its application for use as a wavelength-band selection filter

Yongjun Lim, Seyoon Kim, Junghyun Park, Hwi Kim, and Byoungho Lee*

National Creative Research Center for Active Plasmonics Application Systems, Inter-University Semiconductor Research Center and School of Electrical Engineering, Seoul National University, Gwanak-Gu Gwanakro 599, Seoul 151-744, South Korea

*Corresponding author: byoungho@snu.ac.kr

Received 17 August 2009; revised 17 October 2009; accepted 6 November 2009; posted 6 November 2009 (Doc. ID 115784); published 19 November 2009

We analyzed and experimentally tested a metal–dielectric composite waveguide structure. After coating the surface of the metal layer in the Kretschmann attenuated total internal reflection configuration with a dielectric layer, we explain the coupling of incident light into the coated layer. After finding the dispersion relationships for the layered media including the metal–dielectric composite waveguide, we can determine a solution for its existance in a complex domain. By inscribing a periodic grating structure in the dielectric layer of the metal–dielectric composite waveguide, we experimentally verify the coupling of incident light on the metal–dielectric composite waveguide structure and propose its application for use as a wavelength-band selection filter. © 2009 Optical Society of America

OCIS codes: 240.6680, 230.7400, 230.7408.

1. Introduction

Transferring and coupling light to a target structure is a fundamental issue in optics. Previous studies have reported that efficient coupling of light can be achieved when it is coupled to surface plasmons that are present at the metal–dielectric interface [1–3]. With the Kretschmann configuration, which is widely used for the excitation of surface plasmons, the inherent momentum mismatch between surface plasmons and light in free space can be matched [4]. Based on this fundamental configuration, various applications such as sensors, filters, waveguide holograms, and lithographic methods have been proposed [5–13]. By adding a dielectric layer to the surface of the Kretschmann configuration, it is possible to constitute a metal–dielectric composite waveguide (MDCW) structure, where the prism can serve as a waveguide coupler [13,14]. Here, light emerging from the prism can be efficiently coupled at a few selected incident angles that exceed the critical angle for the system, meaning that the filtering property is included. However, the issue related to the difference between the surface plasmon mode and the waveguide mode, when the dielectric layer is attached to the metal surface of the Kretschmann structure, requires additional clarification [11,15]. This was partially analyzed in a previous paper by comparing the wavenumber of the coupled light calculated using the extended transfer matrix method [13].

To analyze the difference between the two modes present in the MDCW, it is fundamentally necessary to find a dispersion relation in stratified media and to find the corresponding solution in the complex domain [16,17]. In this approach we used a Kuhn algorithm to numerically solve the dispersion relationships including the MDCW slab. In addition, the efficient filtering properties of the MDCW can be used as a wavelength-band selection filter in free space by inserting an outcoupler grating into the MDCW. To use the MDCW with an outcoupler grating as a wavelength-band selection filter in free space, it is necessary to evaluate the properties of both the waveguide mode and the

0003-6935/10/070A23-07$15.00/0

surface plasmon mode under conditions of illumination by broadband white light. Since the waveguide mode and the surface plasmon mode are generally estimated and considered under conditions of monochromatic illumination, the spectral response of each mode for polychromatic illumination has not been appropriately demonstrated. In addition, previously reported research on multimode formation in the MDCW has largely been concerned with numerically evaluated results. Therefore, they usually fail to detect the difference between the filtering properties of each mode. In this approach, the material dispersion of the dielectric layer of the MDCW is taken into consideration. Hence, after we appropriately choose the thickness of the dielectric layer of a MDCW that has both a waveguide mode and a surface plasmon mode, it becomes possible to experimentally demonstrate and compare their individual filtering properties.

In this approach, the coupling of incident p-polarized light into our proposed MDCW configuration can be demonstrated, based on the dispersion relationships. After designing and fabricating an outcoupler grating, coupling light into the MDCW is demonstrated, and a feasibility test of the MDCW with a grating for a wavelength-band selection filter is carried out. A comparison of a surface plasmon mode based filter with a waveguide mode based filter is also experimentally demonstrated under illumination with broadband light.

2. Analysis and Experimental Findings for Coupling Incident Light into Four-Layer Media

A. Dispersion Relationships

Adding a dielectric layer to the metal surface in the Kretschmann attenuated total internal reflection configuration can change the resonance conditions between the incident light and the surface plasmons, depending on the thickness and the refractive index of the added dielectric material [14]. A schematic diagram of the configuration to be investigated is shown in Fig. 1. Previous studies have shown that adding a dielectric layer with an appropriate thickness can change the number of modes coupled into the target dielectric layer, i.e., a layer of poly(methyl 2-methylpropenoate) (PMMA) [11,13,15]. The schematic diagram shown in Fig. 1 describes our one-dimensional four-layer media including the MDCW slab. Here, for the case of p-polarized light, the magnetic field in each layer can be written as follows:

$$\vec{H}_{y0} = \hat{y} H_{y0} \exp(-jk_{z0}z), \tag{1}$$

$$\vec{H}_{y1} = \hat{y}\{H_{y1}^{+} \exp(jk_{z1}z) + H_{y1}^{-} \exp[-jk_{z1}(z-d_1)]\}, \tag{2}$$

$$\vec{H}_{y2} = \hat{y}\{H_{y2}^{+} \exp[jk_{z2}(z-d_1)] + H_{y2}^{-} \exp[-jk_{z2}(z-d_2-d_1)]\}, \tag{3}$$

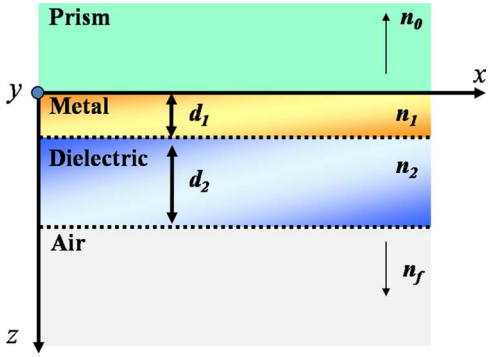

Fig. 1. (Color online) Schematic diagram of the four-layer medium including the MDCW.

$$\vec{H}_{yf} = \hat{y} H_{yf} \exp[jk_{zf}(z-d_2-d_1)]. \tag{4}$$

In Eqs. (1) through (4), the common factors of $\exp[j(k_x x - \omega t)]$ are omitted, where k_x and ω are the x-directional wavenumber and the angular frequency, respectively. Note that, in the prism layer [Eq. (1)], the incident light wave, i.e., the $\exp(jk_{z0}z)$ component, is not considered because the purpose of the investigation is to determine the bound modes in the layered structures. The incident wave could excite the bound modes. The z-directional wavenumber in each layer is presented as follows:

$$k_{z0} = k_0 \sqrt{\varepsilon_0 - (k_x/k_0)^2}, \tag{5}$$

$$k_{z1} = k_0 \sqrt{\varepsilon_1 - (k_x/k_0)^2}, \tag{6}$$

$$k_{z2} = k_0 \sqrt{\varepsilon_2 - (k_x/k_0)^2}, \tag{7}$$

$$k_{zf} = k_0 \sqrt{\varepsilon_f - (k_x/k_0)^2}. \tag{8}$$

By taking the boundary condition into consideration, it is possible to find the following equations at each boundary. For convenience, let $X_i = \exp(jk_{zi}d_i)$, where d_i is the thickness of the metal and the dielectric of the MDCW. At each boundary, for the magnetic field component in the y direction, H_y, and the electric field component in the x direction, E_x, to be continuous, we have the following equation sets.

At the boundary $z = 0$,

$$H_{y0} - H_{y1}^{+} - H_{y1}^{-} X_1 = 0, \tag{9}$$

$$\frac{k_{z0}}{\varepsilon_0} H_{y0} + \frac{k_{z1}}{\varepsilon_1} H_{y1}^{+} - \frac{k_{z1}}{\varepsilon_1} H_{y1}^{-} X_1 = 0. \tag{10}$$

At the boundary $z = d_1$,

$$H_{y1}^{+}X_1 + H_{y1}^{-} - H_{y2}^{+} - H_{y2}^{-}X_2 = 0, \tag{11}$$

$$-\frac{k_{z1}}{\varepsilon_1}H_{y1}^{+}X_1 + \frac{k_{z1}}{\varepsilon_1}H_{y1}^{-} + \frac{k_{z2}}{\varepsilon_2}H_{y2}^{+} - \frac{k_{z2}}{\varepsilon_2}H_{y2}^{-}X_2 = 0. \tag{12}$$

At the boundary $z = d_1 + d_2$,

$$H_{y2}^{+}X_2 + H_{y2}^{-} - H_{yf} = 0, \tag{13}$$

$$-\frac{k_{z2}}{\varepsilon_2}H_{y2}^{+}X_2 + \frac{k_{z2}}{\varepsilon_2}H_{y2}^{-} + \frac{k_{zf}}{\varepsilon_f}H_{yf} = 0. \tag{14}$$

By letting $A_i = \frac{k_{zi}}{\varepsilon_i}$, the above equation sets for determination of a nontrivial solution can be written as follows:

$$\begin{pmatrix} 1 & -1 & -X_1 & 0 & 0 & 0 \\ A_0 & A_1 & -A_1X_1 & 0 & 0 & 0 \\ 0 & X_1 & 1 & -1 & -X_2 & 0 \\ 0 & -A_1X_1 & A_1 & A_2 & -A_2X_2 & 0 \\ 0 & 0 & 0 & X_2 & 1 & -1 \\ 0 & 0 & 0 & -A_2X_2 & A_2 & A_f \end{pmatrix} \begin{pmatrix} H_{y0} \\ H_{y1}^{+} \\ H_{y1}^{-} \\ H_{y2}^{+} \\ H_{y2}^{-} \\ H_{yf} \end{pmatrix} = 0. \tag{15}$$

Accordingly, the solution for Eq. (15) can provide the value of k_x in Eqs. (5) through (8). Since it is difficult to solve Eq. (15) analytically, the Kuhn algorithm is used as an alternate method to obtain the accurate roots of Eq. (15).

B. Solution of the Dispersion Relation by Use of the Kuhn Algorithm

To find a solution that satisfies Eq. (15), we use the Kuhn algorithm, which is adequate to find a root in a complex domain [16,18,19]. When there are roots in the complex domain, performing the Cauchy integral along the contour provides the following equation:

$$S_r = \frac{1}{2\pi j}\oint z^r \frac{f'(z)}{f(z)}\mathrm{d}z = \sum_{i=1}^{n}\phi_i^r, \qquad (r = 0,\ 1,\ 2,\ \ldots,\ n), \tag{16}$$

where ϕ_i represents the root of the analytic function, $f(z)$, and n represents the number of roots. When r in Eq. (16) is zero, the number of roots of ϕ_i can be found, resulting in the following:

$$S_1 = \sum_{i=1}^{n}\phi_i^1, \qquad S_2 = \sum_{i=1}^{n}\phi_i^2,$$
$$S_3 = \sum_{i=1}^{n}\phi_i^3, \ \ldots, S_n = \sum_{i=1}^{n}\phi_i^n. \tag{17}$$

However, since Eqs. (17) include equations of the nth-order degree, it is not easy to solve them in a direct way. The following Newton method can provide a solution for the derived equations [16,18,19]:

$$\begin{cases} \sigma_1 = -(\phi_1 + \phi_2 + \ldots + \phi_n) \\ \sigma_2 = \phi_1\phi_2 + \phi_2\phi_3 + \ldots + \phi_{n-1}\phi_n \\ \qquad\vdots \\ \sigma_n = (-1)^n\phi_1\phi_2\ldots\phi_n \end{cases}, \tag{18}$$

$$\begin{cases} S_1 + \sigma_1 = 0 \\ S_2 + S_1\sigma_1 + 2\sigma_2 = 0 \\ \qquad\vdots \\ S_n + S_{n-1}\sigma_1 + S_{n-2}\sigma_2 + \ldots S_1\sigma_{n-1} + n\sigma_n = 0 \end{cases}. \tag{19}$$

From Eqs. (18) and (19), it is possible to find a solution that gives the root of the analytic function. Bearing in mind our experiments, the simulation result for the structure, composed of an SF10 prism, a 45 nm silver layer, and a PMMA layer with a thickness of 280 nm, is shown in Fig. 2. Under a wavelength of 532 nm, the corresponding refractive indices are, respectively, 1.73, $0.13 + i3.2$, and 1.49. As shown in Fig. 2, the darker the color scale, the easier it is to locate the position of the root of the analytic function. Figure 2 shows that two solutions are possible, the normalized values of which are, respectively, $1.1051 + i0.9899 \times 10^{-7}(\approx 0)$ (left dark spot) and $1.6707 + i0.4675 \times 10^{-2}$ (right dark spot). Hence, with regard to the corresponding propagation length given by the imaginary part of k_x, i.e., $1/(2 \times \mathrm{Im}[k_x])$, the former propagates much farther than the latter. However, the real part of the first solution is low, which makes the coupled light propagate predominantly along the PMMA–air interface. The second mode has an imaginary value of 0.004675, which has an equivalent propagation length of 9.0542 μm, decaying exponentially along the metal–dielectric interface. Thus, the first mode can be regarded as a guided mode and the second as a surface plasmon mode. At these two specific modes, under conditions of monochromatic illumination, the incident light can be coupled into the MDCW, the experimental results for which are shown with the corresponding reflection-dip angles. In addition, our proposed MDCW is a multimode waveguide that is excited by a prism placed on the metal side. Because of the presence of a metallic layer, the loss is caused by

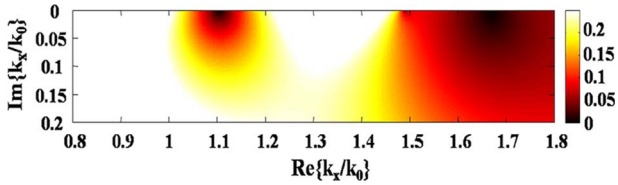

Fig. 2. (Color online) Results of the analytic solution of the dispersion relation given by the Kuhn algorithm.

absorption by the metallic layer. Another source of loss is the radiation toward the prism.

C. Experiments Concerning the Coupling of the Light into the MDCW under Monochromatic Illumination

In this experiment, a second-harmonic Nd:YAG laser with a wavelength of 532 nm was used as the light source. After deposition of a 45 nm Ag film on the SF10 window, a 280 nm PMMA layer was spin coated on the surface of the Ag film. The results for the reflectance measurements and the corresponding simulation results are shown in Fig. 3. It can be readily seen that there are two reflection dips. With regard to the numerical analyses given in Subsection 2.B, one at an angle of 39.5° is the waveguide mode and the other at 75.5° is the surface plasmon resonance mode.

3. Experiments on the MDCW Using an Outcoupler Grating

Here we experimentally verify the coupling of light into our MDCW as well as the filtering characteristics of our MDCW, and an outcoupler grating is designed using a rigorous coupled wave analysis (RCWA). In our proposed configuration, the filtering characteristics are determined by the MDCW and the prism, and the thickness of the dielectric layer of the MDCW determines the mode as well as the number of modes. The designed grating is simply used as an outcoupler grating, which allows the coupled light to emerge from the MDCW.

First, to experimentally identify the coupled lights in the MDCW, we measure the light diffracted by it under monochromatic illumination while decoupling the light in the MDCW with the designed grating. Second, the MDCW for a wavelength-band selection filter is tested under broadband light illumination.

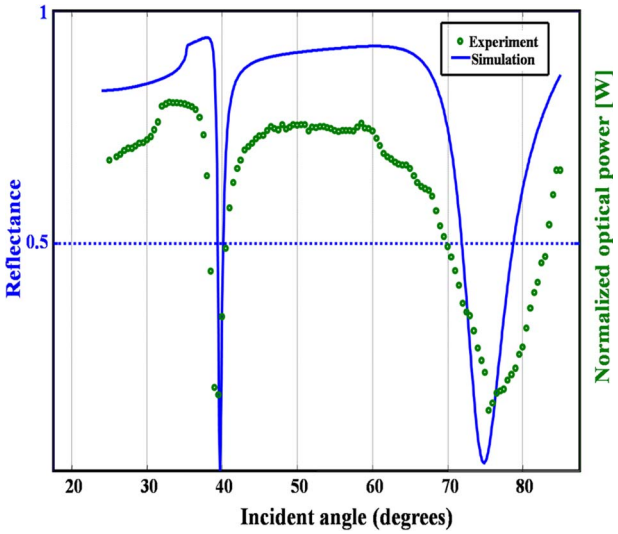

Fig. 3. (Color online) Experimental results for reflectance under illumination by a second-harmonic Nd:YAG laser with a wavelength of 532 nm.

A. Outcoupling of the Light in the MDCW under Monochromatic Illumination

By measuring the diffracted light that emanates from the grating region of the MDCW, the coupled light formed as the waveguide mode and the surface plasmon resonance mode is experimentally investigated. With reference to the design value given by our RCWA, we prepared an outcouler grating to decouple the light in the MDCW.

To experimentally identify the coupled light in the MDCW, we carried out an analysis of the dielectric grating to be inscribed in the MDCW. Figure 4 shows a schematic diagram for the MDCW with an outcoupler grating. As is seen in Fig. 4, we assume that the incident light reaches the outcoupler grating after it propagates through the MDCW. In other words, the outcoupler grating does not diffract the incident light directly but diffracts the light coupled in the MDCW. In our design of the grating, we used a numerical calculation that adopts the RCWA [20–26]. The phase relation between the wavenumber of the MDCW and the dielectric grating wavenumber can be given as follows:

$$k_{\mathrm{MDCW}} = k_0 \sin\theta \pm \frac{2\pi}{\Lambda} q \qquad (q = 0, 1, 2, 3, \ldots), \tag{20}$$

where k_{MDCW}, k_0, θ, and Λ are, respectively, the wavenumber of the mode supported through the MDCW, the free-space wavenumber, the radiation angle of the diffracted light, and the period of the dielectric grating. Integer q represents the diffraction order. Using our RCWA, we chose the period of the grating as 500 nm, the fill factor of which is 0.5.

The scanning electron microscope (SEM) image in Fig. 5 shows the grating structure fabricated by focused ion beam machining, and the size of the fabricated structure is 30 μm (vertical) × 12.5 μm (horizontal). The height of each dielectric grating and its period are, respectively, 280 and 500 nm. The fabricated grating is located in the dielectric layer of the MDCW.

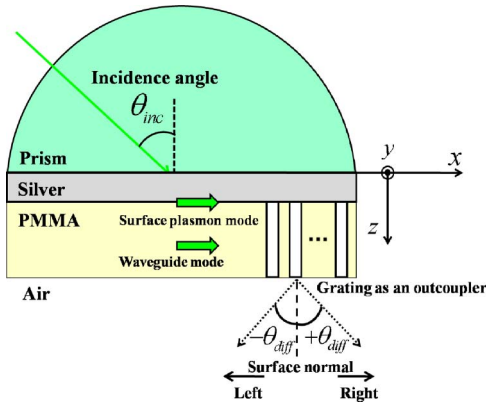

Fig. 4. (Color online) Schematic diagram of the decoupling grating in our MDCW.

With regard to both the values of the two modes given by the Kuhn algorithm and the experimentally obtained reflection-dip angles, we perform a numerical analysis on the diffraction of light that passes through the outcoupler grating in our MDCW. The simulation results with respect to the electric field along the x axis at those two specific modes are shown, respectively, in Figs. 6(a) and 6(b).

In our experiment, with reference to the schematic diagram shown in Fig. 4, we measure the diffracted light that emerges from the inscribed grating. At a waveguide mode excitation angle of 39.5°, the radiation angle of the diffracted light deviates by approximately 3° to the left with respect to the surface normal direction of the MDCW. Two diffracted beams are detected at a surface plasmon resonance angle of 75.5°; one is at 35° to the left of the surface normal direction and the other is 8° to the right. At each reflection dip, we also measure the power of the diffracted beams after placing a lens in front of the power detector to permit the diffracted light to be gathered into the power detector. When the measured input power of the incident light is 1 mW, the powers of the two diffracted lights that emerge from the inscribed grating at each reflection dip are, respectively, 120 and 85 μW.

B. Filtering Properties of the MDCW under Broadband Light Illumination

Here we test the filtering characteristics of each mode in the MDCW. We obtain spectra of the diffracted beam that emanates from the inscribed grating by illumination with a white-light source (LS-F100HS, Osram Korea Corporation, Seoul, South Korea) with a spectral range from 400 to 700 nm. The experimental setup used to measure the bandwidth of the diffracted spectra is shown in Fig. 7. Here we use a relay-optics configuration composed of three lenses so as to have a white-light source with directionality and to make the beam diameter as small as possible.

At two fixed angles, i.e., 39.5° and 75.5°, we measure the filtered spectra of the incident white-light source. When performing this experiment, the large beam diameter of the incident white light could reach the region of the MDCW with the inscribed grating. As a result, this might cause problems in terms of measuring the bandwidth of diffracted spectra at those specific incident angles. However, under the incident angles of 39.5° and 75.5°, by the presence of the grating on the silver film, the propagation constant along the grating–silver interface differs from those of both the surface plasmon mode and the waveguide mode formed in the MDCW. Hence, when the incident light reaches the grating-embedded region, most of the incident light is reflected at those specific angles. This can be simply understood from our simulations on the corresponding reflectance plot. Here we simply consider the material dispersion of the silver in the numerical simulation because the indices of the prism (SF10) and the PMMA vary much less than that of the silver within the wavelength range from 400 to 700 nm. In Figs. 8(a) and 8(b), which show the numerically calculated reflectance, the solid curve shows the reflectance of the incident light that illuminates the grating-embedded region, and the dashed

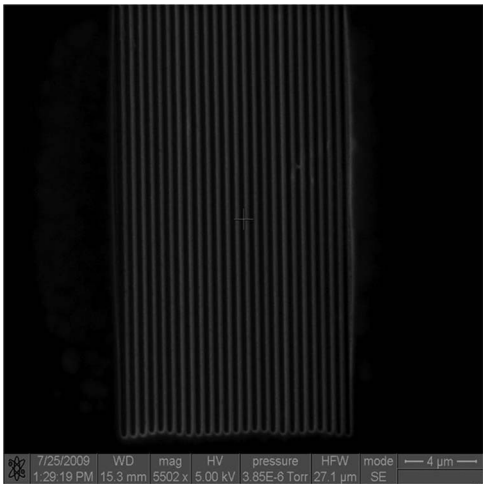

Fig. 5. SEM image of the outcoupler.

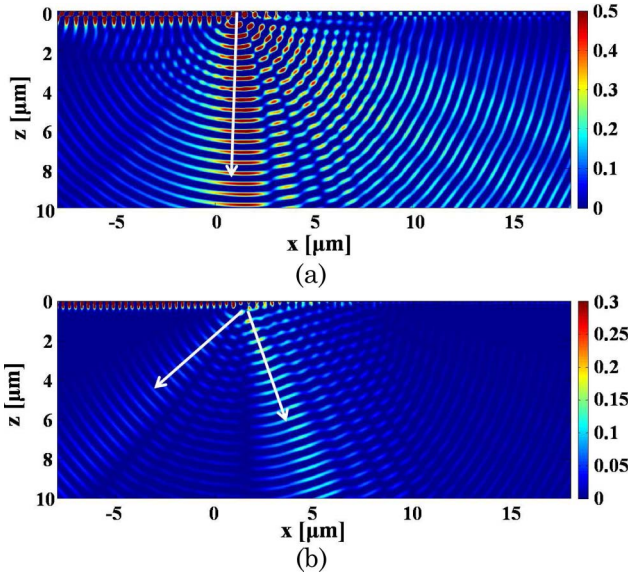

Fig. 6. (Color online) Numerical results for the decoupling grating: (a) the diffracted electric field along the x axis of the waveguide mode and (b) that of the surface plasmon mode.

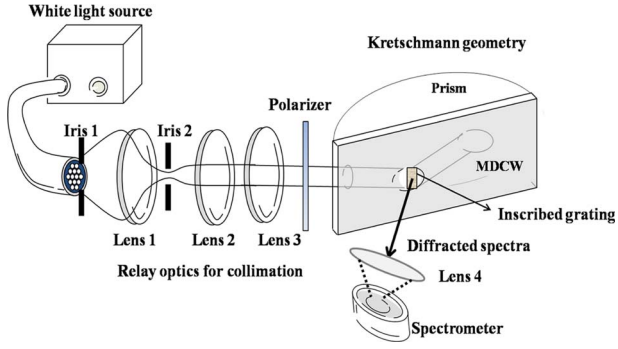

Fig. 7. (Color online) Experimental setup for measuring the filtering properties of the MDCW with the designed grating.

curve with the circles represents the incident light that illuminates the MDCW. As can be seen in Figs. 8(a) and 8(b), the incident light can be largely coupled to the MDCW but not to the region with the grating, because the reflectance at the region with the inscribed grating is quite high. Hence, it is the light coupled into the MDCW that is largely diffracted by the inscribed grating, i.e., incident light can be coupled to the MDCW and, after longitudinal propagation, it can diffract at the grating.

The results for the measured spectra of the input beam and diffracted beam at each angle are shown in Figs. 9(a) and 9(b). The measured spectral widths for the full width at half-maximum (FWHM) are, respectively, 46 and 43 nm; they are expected to be 12 and 43 nm, respectively, according to Figs. 8(a) and 8(b). In addition, the peak values of the diffracted spectra are, respectively, 533 and 534 nm, which are close to the 532 nm wavelength at the minimum reflectance shown in Figs. 8(a) and 8(b).

Bearing in mind that we did not consider the material dispersions of the dielectric layers surrounding the silver layer in Figs. 8(a) and 8(b), their effect can be seen by comparison with our experimental results in Figs. 9(a) and 9(b). When we compare the numerical results shown in Fig. 8(a) with the corresponding experimental results shown in Fig. 9(a), the experimental results for the waveguide mode angle have a wider FWHM than the value given by the simulation results. However, in the case of Figs. 8(b) and 9(b), the FWHM of the surface plasmon mode takes the same value in either case. Thus, it can be seen that the material dispersion of the dielectric layer attached to the silver layer has a greater effect on the diffracted spectra measured at the waveguide mode angle than it does on that at the surface plasmon mode angle. In other words, the surface plasmon based filter based on our MDCW configuration is affected by the material dispersion of the dielectric layer in the MDCW only negligibly, whereas the waveguide mode based filter is vulnerable to the material dispersion of the dielectric layer under broadband white-light illumination.

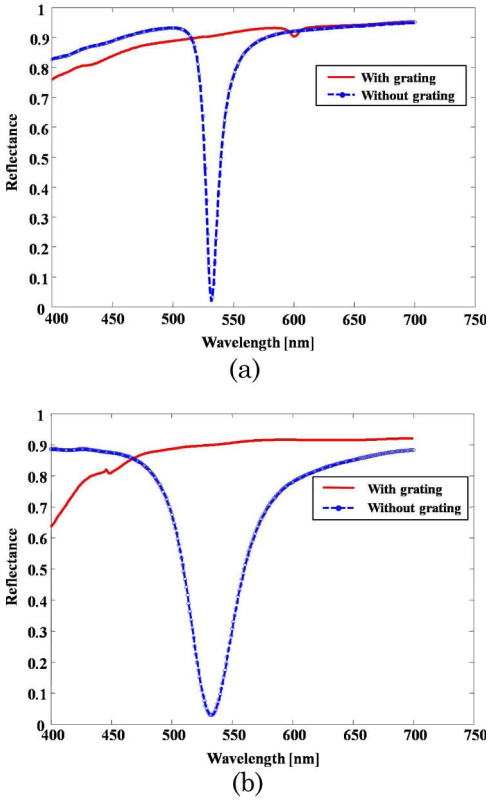

Fig. 8. (Color online) Reflectance of incident white light: the solid curve in each figure represents the reflectance of incident light for the grating-embedded region; the dashed curve indicates the reflectance of the MDCW region without the grating: (a) at the waveguide mode excitation angle and (b) at the surface plasmon resonance angle.

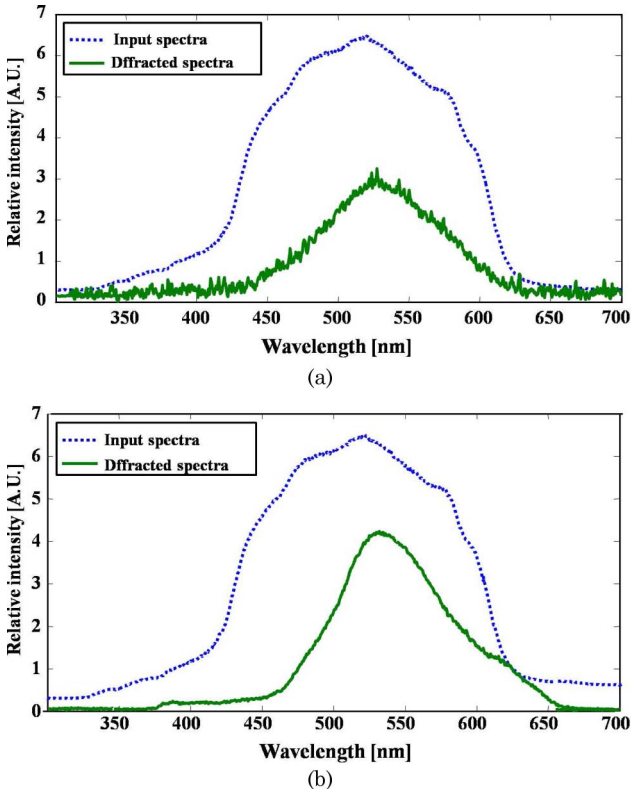

Fig. 9. (Color online) Measured spectra of the bandwidth of the MDCW with the inscribed grating at incident angles of (a) 39.5° and (b) 75.5°.

As can be seen in Figs. 8 and 9, our proposed MDCW with the designed grating has the properties of wavelength-band selection filters. Hence, it would be expected that, by simple adjustment of either the index or the thickness of the dielectric layer of the MDCW, the wavelength-band selection of the inscribed grating could be tuned.

C. Additional Remarks

In our experiment, we should consider the case of the direct coupling of incident light into the grating-embedded region. For this case, the reflection dip occurs at an incident angle of 54° under monochromatic illumination. Similar related phenomenon

was reported in a study of the radiation property of surface plasmon polaritons (SPPs) across dielectric gratings placed on the metal layer in the Kretschmann configuration [7]. Analogous explanations can be made in this case. In our experiment with monochromatic illumination, however, we did not illuminate the region with the grating. Neither did we conduct experiments on the filtering properties under a white-light source at the incident angle of 54°.

4. Conclusion

We have analyzed a metal–dielectric composite waveguide based on the Kretschmann attenuated total internal reflection configuration. The Kuhn algorithm was used to solve the dispersion relationships of our four-layer media, the mode formation of which has been shown numerically. By inserting a dielectric grating analyzed by rigorous coupled wave analysis into the MDCW, we were able to verify the coupling of light into our MDCW both experimentally and numerically. A feasibility test of the potential applications of our device for use as a wavelength-band selection filter was carried out by illumination with a broadband white-light source, and the difference between the surface plasmon mode filter and the waveguide mode filter has been demonstrated.

The authors acknowledge the support of the National Research Foundation and the Ministry of Education, Science and Technology of Korea through the Creative Research Initiative Program (Active Plasmonics Application Systems).

References

1. A. V. Zayats, I. I. Smolyaninov, and A. A. Maradudin, "Nano-optics of surface plasmon polaritons," Phys. Rep. **408**, 131–314 (2005).
2. Z. Chen, I. R. Hooper, and J. R. Sambles, "Grating-coupled surface plasmon polaritons and waveguide modes in a silver–dielectric–silver structure," J. Opt. Soc. Am. A **24**, 3547–3553 (2007).
3. S. Maier and H. Atwater, "Plasmonics: localization and guiding of electromagnetic energy in metal/dielectric structures," J. Appl. Phys. **98**, 011101 (2005).
4. H. Raether, *Surface Plasmons on Smooth and Rough Surfaces and on Gratings.* (Springer-Verlag, 1988).
5. J. Homola, S. S. Yee, and G. Gauglitz, "Surface plasmon resonance sensors: review," Sens. Actuators B **54**, 3–15 (1999).
6. B. Lee, S. Roh, and J. Park, "Current status of micro- and nano-structured optical fiber sensors," Opt. Fiber Technol. **15**, 209–221 (2009).
7. S. Park, G. Lee, S. Song, C. Oh, and P. Kim, "Resonant coupling of surface plasmons to radiation modes by use of dielectric gratings," Opt. Lett. **28**, 1870–1872 (2003).
8. Y. Lim, S. Chung, S. Kim, S. Han, and B. Lee, "Wavelength-band selection filter based on surface plasmon resonance and phase conjugation holography," IEEE Photon. Technol. Lett. **18**, 2532–2534 (2006).
9. Z. Wu, J. Haus, Q. Zhan, and R. Nelson, "Plasmonic notch filter design based on long-range surface plasmon excitation along metal grating," Plasmonics **3**, 103–108 (2008).
10. S. Maruo, O. Nakamura, and S. Kawata, "Evanescent-wave holography by use of surface-plasmon resonance," Appl. Opt. **36**, 2343–2346 (1997).
11. G. Wang, T. Sugiura, and S. Kawata, "Holography with surface-plasmon-coupled waveguide modes," Appl. Opt. **40**, 3649–3653 (2001).
12. X. Guo, J. Du, Y. Guo, and J. Yao, "Large-area surface-plasmon polariton interference lithography," Opt. Lett. **31**, 2613–2615 (2006).
13. Y. Lim, S. Kim, H. Kim, J. Jung, and B. Lee, "Interference of surface plasmon waves and plasmon coupled waveguide modes for the patterning of thin film," IEEE J. Quantum Electron. **44**, 305–311 (2008).
14. I. Pockrand, "Surface plasma oscillations at silver surfaces with thin transparent and absorbing coatings," Surf. Sci. **72**, 577–588 (1978).
15. K. Choi, H. Kim, Y. Lim, S. Kim, and B. Lee, "Analytic design and visualization of multiple surface plasmon resonance excitation using angular spectrum decomposition for a Gaussian input beam," Opt. Express **13**, 8866–8874 (2005).
16. Y. L. Long, and E. K. N. Yung, "Kuhn algorithm: ultraconvenient solver to complex polynomial and transcendental equations without initial value selection," Int. J. RF Microwave Comput.-Aided Eng. **12**, 540–547 (2002).
17. Y. Lim, S. Kim, and B. Lee, "Dispersion relation and its solution using Kuhn algorithm in stratified media accompanying with surface plasmon resonance," in *Pacific Rim Conference on Lasers and Electro-Optics* (Optical Society of America, 2007), paper WF3-3.
18. L. Delves and J. Lyness, "A numerical method for locating the zeros of an analytic function," Math. Comput. **21**, 543–560 (1967).
19. T.-Y. Li, "On locating all zeros of an analytic function within a bounded domain by a revised Delves/Lyness method," Siam (Soc. Ind. Appl. Math.) J. Numer. Anal. **20**, 865–871 (1983).
20. M. Moharam and T. Gaylord, "Rigorous coupled-wave analysis of planar-grating diffraction," J. Opt. Soc. Am. **71**, 811–818 (1981).
21. M. Moharam, E. Grann, D. Pommet, and T. Gaylord, "Formulation for stable and efficient implementation of the rigorous coupled-wave analysis of binary gratings," J. Opt. Soc. Am. A **12**, 1068–1076 (1995).
22. G. Granet and B. Guizal, "Efficient implementation of the coupled-wave method for metallic lamellar gratings in TM polarization," J. Opt. Soc. Am. A **13**, 1019–1023 (1996).
23. P. Lalanne and G. M. Morris, "Highly improved convergence of the coupled-wave method for TM polarization," J. Opt. Soc. Am. A **13**, 779–784 (1996).
24. E. Silberstein, P. Lalanne, J. P. Hugonin, and Q. Cao, "Use of grating theories in integrated optics," J. Opt. Soc. Am. A **18**, 2865–2875 (2001).
25. Q. Cao, P. Lalanne, and J. P. Hugonin, "Stable and efficient Bloch-mode computational method for one-dimensional grating waveguides," J. Opt. Soc. Am. A **19**, 335–338 (2002).
26. H. Kim, I. Lee, and B. Lee, "Extended scattering-matrix method for efficient full parallel implementation of rigorous coupled-wave analysis," J. Opt. Soc. Am. A **24**, 2313–2327 (2007).